

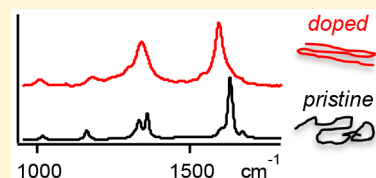
Charge Transfer Doping Induced Conformational Ordering of a Non-Crystalline Conjugated Polymer

Alan K. Thomas, Ryan Johnson, Benjamin W. Stein,[†] Martin L. Kirk,[‡] Hua Guo,[‡] and John K. Grey^{*‡}

Department of Chemistry and Chemical Biology, University of New Mexico, Albuquerque, New Mexico 87131, United States

Supporting Information

ABSTRACT: Charge transfer doping of a nominally disordered conjugated polymer induces long-range conformational ordering (stiffening) of backbone segments. Addition of [2,3-dichloro-5,6-dicyano-*p*-benzoquinone (DDQ) to dilute solutions of poly[2-methoxy-5-(3',7'-dimethyloctyloxy)-1,4-phenylenevinylene] (MDMO-PPV) results in quantitative charge transfer in the ground electronic state of the polymer. Following charge (hole) injection, greater MDMO-PPV monomer coplanarity is evident in electronic, Raman, and electron paramagnetic resonance (EPR) spectra over a broad range of dopant loadings. New transitions emerge at lower energies with spectral patterns distinct from pristine materials but closely resemble minority low energy conformers selectively that can be prepared by careful control of processing conditions. We further demonstrate that characteristic Raman patterns of PPV systems actually contain signatures of a minority ordered form that interacts preferentially with the dopant. Subsequent additions of dopant also show that most chains convert into the low energy form. This notion is consistent with greater backbone planarity and, hence, lower torsional reorganization energies required to access the cation form. Preresonant excitation of the emergent red-shifted optical transition reveals long overtone-combination progressions due to enhanced electronic delocalization along planarized backbone segments and diminished coupling the surroundings. We propose that planarity enhancements from doping also lead to the eventual formation of spinless bipolarons, evident from EPR spectra. Facile charge transfer doping induced conversion into the ordered MDMO-PPV conformer suggests that better control of polymer conformations and carrier levels could be harnessed to improve charge and energy transport efficiency in optoelectronic devices.



INTRODUCTION

The use of strong electron acceptor molecules to electrically dope conjugated organic materials in their ground electronic state via charge transfer is an attractive approach for tuning carrier densities for various optoelectronic applications.^{1–4} This process is most commonly undertaken in solutions prior to casting into films, which offers greater flexibility and potential tunability of desired electrical properties. However, structural changes induced by doping tend to alter film morphological characteristics significantly from those of pristine films necessitating new processing approaches to achieve reliable control of electrical properties.⁵ In addition, doping also gives rise to new multiparticle charged species and interactions, such as bipolarons, resulting in more opportunities for understanding charge transport pathways and charge interactions.^{6–9}

Ideally, a free charge carrier (polaron) is generated in a localized region of the polymer chain (segment) for every charge transfer event with an acceptor but this is seldom realized in practice.¹⁰ At the simplest level, the choice of suitable electron acceptors is typically guided by consideration of frontier energy level offsets (i.e., acceptor ~ LUMO vs donor ~ HOMO). However, this pure electronic view has had limited success in determining doping efficacies, namely, the amounts of free carriers generated per dopant added. For example, measured free charge carrier levels in thin films are often far below than those expected based on the amount of dopant added per monomer unit,¹¹ and carrier levels typically saturate

after a characteristic loading. These deviations are usually attributed to nonquantitative charge transfer, disorder-induced charge trapping in the solid state, and dopant preassociation.^{12–15} Molecular structure factors and more detailed theoretical insights are becoming available, which have improved design strategies of charge transfer doping and charge transport.^{13,16–22}

In addition to specific interactions with polymer backbone moieties, the extended conformational properties and aggregation also have a profound impact on charge transfer doping efficiency and subsequent charge transport. Recent work from our group has concentrated on the roles of conformational order and polymorphism on determining charge transfer doping efficiency.^{15,19} In particular, conformations capable of adopting high monomer coplanarity in self-folded aggregate-type structures become quantitatively doped whereas chains of lower order (e.g., regioregularity) form charge transfer complexes.¹⁹ Other work along these lines has focused on the effect of solvents in regulating preaggregation of semi-crystalline polymers as well as cocrystallization of ionized donors and acceptors in the solid phase, which has shed new light on the structural factors dictating doping outcomes.²³ We expand on this theme herein by investigating molecular-level

Received: September 3, 2017

Revised: October 9, 2017

Published: October 9, 2017

polymer–dopant interactions and the extent of structural and conformational rearrangement following a charge transfer event.

Virtually all of the current effort involved in studying conjugated polymer charge transfer doping has been directed toward crystalline systems capable of forming extended π -stacked aggregate networks. Even short-range crystallinity has enabled the use of sensitive scattering and diffraction based characterization tools that have proven effective for resolving changes in aggregated regions of the material upon charge transfer.²⁴ For example, benchmark systems, such as poly(3-hexylthiophene) (P3HT), can be electrically doped in the ground electronic state by adding small amounts of the strong electron acceptor, F₄-TCNQ.^{11,25,26} Despite expected quantitative charge transfer with F₄-TCNQ, it has been estimated that only ~5% or less of dopant additives actually result in free charge carriers (hole polarons) on P3HT chains.^{11,27} The current consensus is that only aggregates become doped while lesser-ordered (amorphous) chains form bound complexes with the ionized dopant.¹⁰ Furthermore, for polymer chains that become doped, there is a characteristic stiffening of the backbone due to quinoidal distortions leading to spectral signatures resembling ordered aggregates.¹⁵ More recently, Neher and co-workers investigated the effect of solvent on P3HT doping characteristics and reported that preaggregation in solution (viz. higher boiling point solvents) limited doping efficiencies and resulting conductivities of thin films.²³

Unfortunately, it is considerably more difficult and less reliable to apply diffraction-based tools to study charge transfer doping of nominally disordered polymers.²⁸ In this case, ordered segments are in much lower abundance and there is often no registry between ordered segments, e.g., π -stacking in polymer aggregates. Here, we use combinations of one- and two-photon spectroscopies to examine how intrinsic conformational qualities influence charge transfer doping and subsequent structural distortions in the ground and excited electronic states of a noncrystalline polymer. Solutions of poly-[2-methoxy-5-(3',7'-dimethyloctyloxy)-1,4-phenylenevinylene] (MDMO-PPV) are doped in the ground electronic state by adding [2,3-dichloro-5,6-dicyano-*p*-benzoquinone (DDQ), a strong π -electron acceptor. New, red-shifted electronic absorption transitions emerge immediately upon addition of DDQ consistent with the creation of ionized MDMO-PPV and dopant forms although spectra are congested because of overlapping transitions in the same energy range. We demonstrate that the unique signatures of doped and undoped forms can be resolved in addition to new evidence of ordered, minority conformers that act as precursors for the doped MDMO-PPV variant.

Despite the noncrystalline nature of MDMO-PPV, multiple stable conformers exist (similar to other alkoxy-PPV derivatives) that have been investigated extensively using single molecule spectroscopy.^{29,30} Bimodal distributions of so-called “red” and “blue” emitting forms corresponding to ordered and solution-like (amorphous) segments, respectively, have been isolated and the amounts can be controlled by choice of preparation conditions (solvent) and polymer molecular weight. The low energy “red” form has been assigned as minority emissive traps (as little as one segment per chain) that are populated chiefly by excitation energy transfer from more plentiful, higher energy “blue” chromophores.^{29,30} Although strong fluorescence quenching forbids direct investigation of doping efficacies of MDMO-PPV conformers in solution and

solid phases, we use resonance Raman spectroscopy to show that doping occurs preferentially for the ordered conformation. As doping levels increase, there is a greater stiffening (ordering) of neighboring segments whereby nearly all chains convert to this form, which is consistent with findings from theoretical simulations and electron paramagnetic resonance (EPR) spectroscopy of MDMO-PPV/DDQ blends. Overall, we find a remarkable similarity between the responses of crystalline and noncrystalline polymers to charge transfer doping, namely, characteristic ordering of the backbone. This result suggests a possible universal design approach for controlling doping outcomes via fine-tuning of structural and conformational characteristics regardless of the ability to form long-range crystalline domains.

■ EXPERIMENTAL SECTION

Sample Preparation and Characterization. MDMO-PPV was obtained from Aldrich (MW ~ 35 000 g/mol, PDI = 2.1) and used without further purification. MDMO-PPV solution samples were dissolved in dry chlorobenzene (2 mg/mL) in a circulating nitrogen glovebox under gentle heating. Solutions of [2,3-dichloro-5,6-dicyano-*p*-benzoquinone (DDQ, Aldrich) (0.5 mg/mL) were prepared under similar conditions and combined with MDMO-PPV over a range of w/w ratios. Typical MDMO-PPV/DDQ loading ratios used spanned between 1:0.05 and 1:2 w/w. The relatively large PDI of MDMO-PPV makes it difficult to estimate the exact number of DDQ dopants per monomer units but we project this to be approximately 200 and 5 monomer units per DDQ molecule added, respectively. Thin films were deposited from blend MDMO-PPV/DDQ solutions on rigorously cleaned glass coverslips there were sealed with an aluminum overcoating by thermal deposition under high vacuum for Raman measurements. Optical absorption spectra of MDMO-PPV/acceptor films were measured on a Varian CARY spectrometer immediately following deposition. Raman spectra were recorded using a home-built confocal microscope spectrometer for excitation wavelength spanning ~450–650 nm described in detail previously.³¹ Off resonance Raman spectra of thin films were measured using 780 nm light with a dispersive spectrometer (Thermo-Nicolet). Resonance Raman excitation profiles were generated using the same microscope system equipped with a home-built sapphire objective as an external intensity standard.³² EPR data were collected at X-band (9.3 GHz) using a Bruker EMX spectrometer with associated Bruker magnet control electronics and microwave bridges. The EPR spectra of doped MDMO-PPV degassed solutions and thin films were recorded at several temperatures ranging from ~5 up to 300 K, and all measurements were made on samples held under a dry nitrogen environment to avoid oxygen and moisture related degradation. Low-temperature spectra were collected using an Oxford Instruments liquid helium flow cryostat and an Oxford Instruments temperature controller.

Theoretical Calculations. Density functional theory (DFT) calculations were performed using the B3LYP hybrid functional with the atom-pairwise dispersion corrections of Grimme et al.³³ and utilizing the Becke and Johnson damping scheme.³⁴ The neutral and anionic forms of DDQ as well as neutral and cationic MDMO-PPV model monomer system were modeled to ascertain bond-length changes due to complexation interactions and understand their spectroscopic signatures. MDMO-PPV analogues use the shorter methoxy groups in place of the longer branched alkoxy side chain in

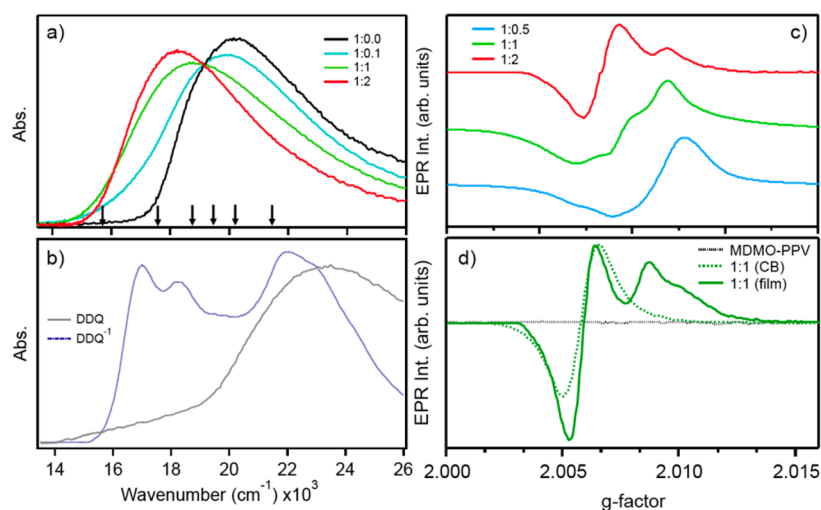


Figure 1. (a) Absorption spectra of MDMO-PPV/DDQ blend thin films at several loadings. Raman excitation energies, *vide infra*, are depicted by downward arrows. (b) Absorption spectra of pristine DDQ and DDQ⁻ solutions. (c) EPR spectra of MDMO-PPV/DDQ blends measured at 4 K. (d) Comparison of pristine MDMO-PPV and DDQ blends (1:1 w/w) in thin film and chlorobenzene solution measured at 300 K.

order to expedite simulations. For both molecules, Ahlrichs Def2-TZP basis sets³⁵ were utilized with p and 2d polarization functions and s and sp dispersion functions on H and main group atoms, respectively. We also explore the effect of MDMO-PPV chain lengths (i.e., monomers) although a smaller basis set was used in which only p and 2d polarization functions on H and main group atoms, respectively, was used. To speed the HF evaluation of exchange, resolution of the identity (RI) for both the exchange and Coulomb integrals and the chain-of-spheres (COSX) approximations were used.³⁶ Raman spectra were simulated using the ORCA computational suite.

RESULTS AND DISCUSSION

Figure 1a shows absorption spectra of MDMO-PPV thin films spin-cast from solutions with varying amounts of DDQ added (absorption spectra of chlorobenzene solutions are included in the Supporting Information). A new transition centered at $\sim 18\,395\text{ cm}^{-1}$ (2.28 eV) becomes apparent in the vicinity of the red edge of the π - π^* singlet exciton band of pristine MDMO-PPV ($\sim 20\,300\text{ cm}^{-1}$, 2.52 eV). As DDQ content increases, the band centered at 2.28 eV grows at the expense of the 2.52 eV band and a characteristic isosbestic point is apparent at $\sim 19\,200\text{ cm}^{-1}$ (2.38 eV) indicating the presence of two structurally distinct species. The emergence of a new red-shifted transition is consistent with a quantitative charge transfer event upon contact between MDMO-PPV segments and DDQ dopants,³¹ consistent with the integer charge transfer model.¹¹ However, one-photon absorption spectra of doped polymer blends are usually comprised of overlapping and inhomogeneously broadened transitions making it difficult to definitively ascertain directly whether injected charges exist as free carriers.

DDQ was next doped with ferrocene to generate DDQ⁻ to further resolve the nature of the emergent red-shifted absorption transition and spectra of both pristine and ionized forms of DDQ are displayed in Figure 1b. Upon formation of DDQ⁻, a new line shape appears with an electronic origin energy (E_{0-0}) of $\sim 17\,070\text{ cm}^{-1}$ (2.12 eV) and a partially resolved vibronic progression of $\sim 1240\text{ cm}^{-1}$ corresponding to excited state distortions along CC normal modes (*vide infra*). Spectral line widths are narrower for the DDQ⁻ band

compared to the new red-shifted band observed in the MDMO-PPV/DDQ blend (i.e., ~ 750 vs $\sim 1900\text{ cm}^{-1}$, respectively). Despite that significant overlap exists between and MDMO-PPV/DDQ blend absorption line shapes, the lack of resolved vibronic structure in the new red-shifted line shape suggests minor contributions from the DDQ⁻ species. We estimate the molar absorptivity of the DDQ⁻ absorption transition to be $\sim 1 \times 10^4\text{ M}^{-1}\text{ cm}^{-1}$ at the absorbance maximum (E_{0-0}), which is much smaller than that of PPV derivatives in same molecular weight range ($\sim 10^5\text{ M}^{-1}\text{ cm}^{-1}$ or greater). Instead, we posit that the emergent transition in Figure 1a is dominated by MDMO-PPV/MDMO-PPV⁺ character.

Comparison of spectral features in Figure 1a with those of related polymer blends with other strong electron acceptors also reveal patent differences. For example, Bruevich et al. investigated blends of MEH-PPV with 2,4,7-trinitrofluorenone (TNF) as an acceptor and observed weak and broadened transitions on the red edge of the pristine polymer absorption line shape for similar loadings as those used here.³⁷ Although TNF has similar qualities as DDQ (i.e., electron affinities) this result suggests that injected holes cannot escape the Coulombic attraction of the ionized dopant and become trapped in a bound charge transfer complex.^{38,39} On the other hand, our results suggest that either free hole polarons or holes that interact weakly with the dopant anion are created when MDMO-PPV chains are doped with DDQ.

EPR spectra of MDMO-PPV/DDQ blends provide a convenient way to probe the nature of injected carriers and the effects of doping that are not available from one-photon electronic absorption spectra. Figure 1c shows 4K EPR spectra of blend thin films using loadings similar to those presented in the electronic absorption spectra (Figure 1a). For comparison, MDMO-PPV/DDQ (1:1 w/w) solution and thin film EPR spectra were also measured at 300 K and these data are shown in Figure 1d. No discernible signal is observed in either the pristine solid material or their precursor solutions demonstrating that all resonances arise because of doping. EPR spectra of MDMO-PPV/DDQ thin films measured at 4K display evidence for the presence of two overlapping EPR transitions that change in relative intensity depending on DDQ loading and temper-

ature. As DDQ concentrations increase, the 4 K spectra shift from a dominant larger g -value resonance ($g \sim 2.0085$) to one possessing a smaller g -value ($g \sim 2.0065$) that is closer to the free electron g -value ($g = 2.0023$). Hyperfine coupling and g -tensor anisotropy may be evident in spectra at smaller loadings ($<1:2$ w/w) but is difficult to fully resolve at X-band frequencies and will not be considered further. The assignment of the ~ 2.0065 (3426 G) resonance to the DDQ anion (DDQ^{-1}) and the ~ 2.0085 (3420 G) resonance to the MDMO-PPV⁺ hole polaron is supported by their similarity to recently reported EPR spectra of a long-lived photoinduced charge transfer species in water-soluble polyelectrolytes with pendant fullerene acceptors.⁴⁰

At liquid helium temperatures, the observed decrease in intensity of the $g \sim 2.0085$ MDMO-PPV⁺ hole polaron resonance, coupled with an increase in intensity for the DDQ^{-1} anion radical as a function of increased loadings is consistent with the initial formation of free hole polarons at low dopant concentrations that convert to spinless hole bipolarons as the hole concentrations increase. The room temperature EPR data for the 1:1 film sample also shows the same two resonances (Figure 1d), but with different intensities compared with the 4 K data set at the same dopant loading. This observation is consistent with a perturbation that results in different relative populations of spinless bipolarons and free hole polarons as a function of temperature. This effect may indicate that entropic effects are at play, which can affect these relative populations through geometric distortions that affect the relative planarity of MDMO-PPV⁺ as a function of dopant concentration, with more planar geometries favoring the formation of spinless bipolarons.¹⁹ Thus, the lower observed intensities of the MDMO-PPV⁺ contribution with larger DDQ loading most likely derives from enhanced polaron delocalization along segments of greater coplanarity, allowing the generated polarons to combine and form spinless bipolarons. Similar suggestions of charge transfer-induced planarity have also been made for MEH-PPV/TNF blends and we explore this proposed structural change in more detail below using Raman spectroscopy.³⁷ This is interesting since it suggests that the effective concentration of spin carriers can be modified by small structural changes that drive the doped polymer between paramagnetic and diamagnetic states as a function of temperature or the nature of the matrix, *vide infra*. In support of this assertion, we note that there is no EPR evidence for free hole polarons in our room temperature solution samples with 1:1 MDMO-PPV/DDQ loadings (Figure 1c). Interestingly, this indicates that either a more planar polymer geometry exists in solution or dynamic structural effects are present that result in the formation of spinless bipolarons.

It is also useful to note that polymer chains of low regioregularity typically form bound charge transfer complexes due to the inability of the injected holes to delocalize from the charge transfer site. We do not observe any EPR signals from these species, which should be present if the electron and hole spins are uncoupled. This behavior can be rationalized in terms of disorder-induced localization of the injected hole (e.g., large torsional displacements) that limit exciton and charge migration lengths. In an earlier study, this effect was investigated using P3HT samples of varying regioregularity where it was found that only the chains of high regioregularity had appreciable levels of free carriers (i.e., large EPR spin densities).¹⁵ Otherwise, charge transfer complexes exhibit weak and broadened absorption lineshapes, which are also not

observed in our samples. To help understand the electronic factors governing branching ratios of free (uncoupled) polarons and spinless bipolarons, we consider the nature of the interactions mediated by the chain structural qualities. First, formation of a spinless bipolaron (open shell singlet) can result due to superexchange coupling between the hole and the electron. Assuming a pairwise exchange Hamiltonian for two coupled spins ($H = -2JS_1S_2$) and antiferromagnetic exchange coupling, the triplet will not be appreciably populated for $k_B T/J < \sim 0.3$. This corresponds to a conservative estimate of $J > 700 \text{ cm}^{-1}$ at 300 K (see Supporting Information). This scenario would correspond to the strong superexchange limit with the spins being in close proximity to one another as expected due to the low dielectric environment of polymeric materials.

The spectroscopic trends presented thus far are consistent with a greater fraction of the ordered MDMO-PPV phase induced by charge transfer doping and the polaronic character of injected holes. Moreover, there is a similarity between the new, red-shifted absorption feature in Figure 1a and absorption line shapes of PPV derivatives deposited from high boiling point solvents (see Supporting Information) as well as those from samples with low polydispersity. Most recently, Koehler and Bässler demonstrated interconversion from the dominant amorphous form to the ordered (red) form in MEH-PPV dispersed in glassy hosts via a second order phase transition at ca. 200 K.⁴¹ This transition requires cooperativity in alkoxy side group packing leading to aggregation even though intermolecular backbone π - π interactions are weak. Excitons of the MEH-PPV red phase have predominant intrachain character where most of the emission intensity is concentrated in the E_{0-0} transition.

We now propose a similar ordering of MDMO-PPV chains occurs in the presence of DDQ whereby charge injection by DDQ increases quinoidal character and therefore greater monomer coplanarity. In a previous report, we examined charge transfer interactions in MDMO-PPV blends with various electron acceptors and observed evidence of charge transfer induced ordering of the polymer backbone.³¹ This structural change was most apparent from resonance Raman spectroscopy that showed long overtone progressions. We investigate these features in more detail to determine the nature of injected carriers and the specific role of structure in dictating doping efficiency. Preresonance Raman spectroscopy is now used to probe the structural origins of the new red-shifted absorption transition in MDMO-PPV/DDQ blends and unravel the structural qualities of the chromophore.

Figure 2 shows Raman spectra of MDMO-PPV/DDQ blends with varying DDQ loading (similar to absorption spectra in Figure 1a) generated using 780 nm light ($12\,820 \text{ cm}^{-1}$, 1.59 eV). As the DDQ loading increases, we observe a redistribution of intensities involving the dominant MDMO-PPV CC symmetric stretching skeletal vibrations in the range of ~ 1550 – 1625 cm^{-1} and ~ 1280 and 1310 cm^{-1} corresponding to phenylene C=C stretching character and inter-ring stretches, respectively. Most notably, large relative intensity gains of the ~ 1280 and 1555 cm^{-1} are observed that appear as shoulders on the ~ 1310 and 1580 cm^{-1} modes, respectively, in the pristine material and eventually dominate the Raman pattern at large DDQ loadings ($>1:1$ w/w). Interestingly, line widths of the emergent ~ 1280 and $\sim 1555 \text{ cm}^{-1}$ modes are broader compared to the corresponding higher frequency ~ 1310 and 1580 cm^{-1} modes in the pristine MDMO-PPV Raman pattern (i.e., ~ 40 vs $\sim 20 \text{ cm}^{-1}$, respectively). We also

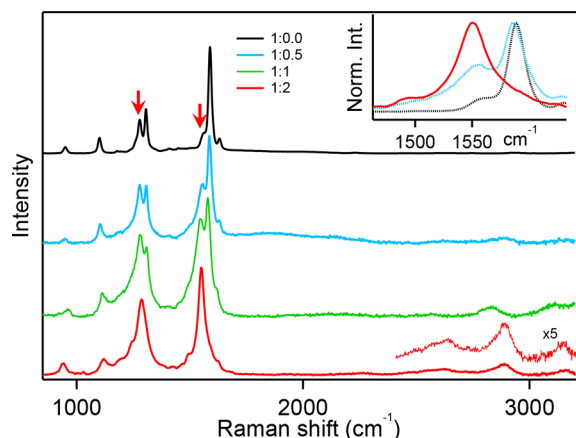


Figure 2. Preresonant Raman spectra of MDMO-PPV/DDQ thin films ($\lambda_{\text{exc}} = 780 \text{ nm}$). Characteristic Raman bands from the ordered form are highlighted as red downward arrows. Inset: blowup of the main CC stretching mode region ca. $1550\text{--}1560 \text{ cm}^{-1}$.

observe red-shifts by $\sim 15 \text{ cm}^{-1}$ for all skeletal vibrations over the entire DDQ loading range that become more appreciable with larger loadings. Previous Raman spectroscopic investigations of PPV systems have assigned the $\sim 1555 \text{ cm}^{-1}$ transition as a symmetric inter-ring $\text{C}=\text{C}$ stretch with significant vinylene stretching character.^{8,42,43} Doping with sodium (i.e., n-doping as opposed to p-doping here) also produces similar trends as shown in Figure 2, namely, a redistribution of CC stretching intensities toward this mode.⁴⁴

The appearance of a distinct red-shifted absorption spectrum in Figure 1 in addition to the pronounced intensity redistributions of the dominant CC backbone stretching modes in preresonance Raman spectra, are consistent with injected hole polarons delocalized along MDMO-PPV segments. Furthermore, the apparent conversion from the typical lineshapes in the pristine material to a lower energy form also indicates that a large fraction of MDMO-PPV segments become planarized upon charge transfer doping. Because the ~ 1280 and $\sim 1555 \text{ cm}^{-1}$ mode intensities exhibit rapid growth

with larger DDQ loadings, we putatively assign these as signatures of the minority ordered form of MDMO-PPV. As more holes are injected, it is apparent that adjacent segments also experience stiffening, which is expected with increased quinoidal character. This effect gives the appearance of creating more of the ordered MDMO-PPV phase similar to temperature-induced phase transitions, which also explains DDQ loading-dependent trends from preresonant Raman spectra in Figure 2.

Similar doping-induced ordering effects were also observed in dilute solutions of P3HT doped with $\text{F}_4\text{-TCNQ}$, which appear as the J-aggregate type of absorption line shape. In this case, only chains of high regioregularity became doped (EPR-active) whereas chains of low regioregularity formed bound charge transfer complexes (EPR silent).¹⁵ Corresponding electronic absorption spectra revealed significant doping-induced aggregation in the former due to greater rigidity of chains with substantial quinoidal character.¹⁵ To further understand how doping affects structural rearrangements of the polymer backbone, we performed theoretical simulations of MDMO-PPV surrogates in the presence of DDQ. Figure 3 shows predicted bond length changes (\AA) before (black) and after (red) complex formation between an MDMO-PPV monomer surrogate and DDQ. A significant reduction in bond lengths is observed for CC double bonds and, likewise, increases for nominal CC single bonds for the pristine benzoid structure. This behavior supports our assignment of increased quinoidal character and is consistent with spectroscopic data presented earlier. Increases in bond lengths for nominal CC double bonds in the DDQ anion in addition to bond length increases for the carbonyl groups are also consistent with quantitative doping.

We next explore the effect of increasing backbone length (number of monomer repeat units) on the degree of charge transfer. If injected charges induce monomer coplanarity as expected with greater quinoidal character, then larger and more planarized segments should provide further impetus for charge injection. Figure 4 shows Lowdin charge transfer integrals calculated from a single MDMO unit up to six repeat units.

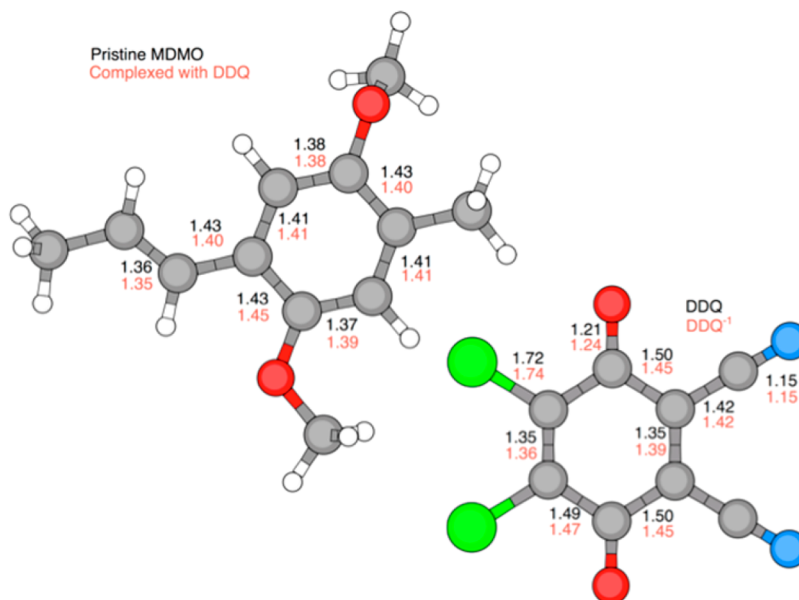


Figure 3. Bond lengths of an MDMO-PPV monomer unit from an oligomer structure and DDQ before (black) and after (red) contact.

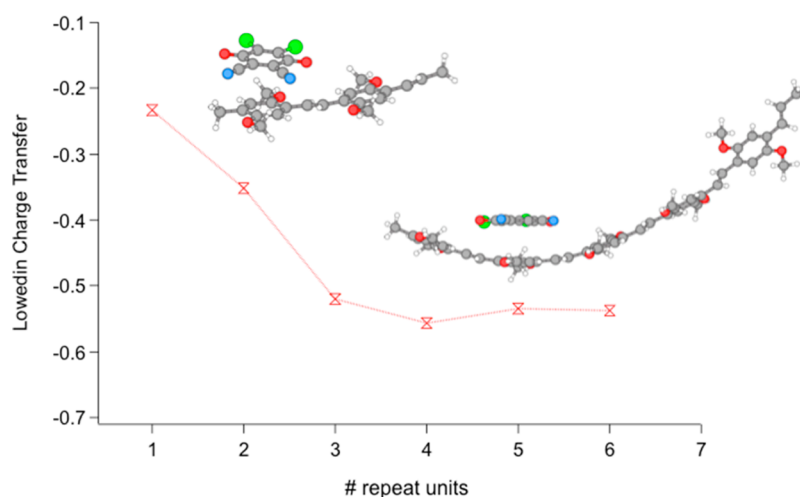


Figure 4. Lowedin charge transfer as a function of MDMO oligomer length.

Representative structures are shown (e.g., 2-mer and 5-mer) and the degree of charge transfer is indeed observed to increase with oligomer length. This result is consistent with the view that enhanced planarization favors greater charge delocalization. Longer chains exhibit a pronounced bending around the ionized dopant although coplanarity between segments does increase. This bending effect probably arises from the fact that the large branched alkoxy side groups of MDMO-PPV are replaced by shorter methoxy groups in the simulations. The longer alkoxy side chains are expected to oppose this type of distortion due to the increased steric hindrance.

Earlier Raman spectroscopic studies of doping in PPV systems used changes in the Raman intensities and frequencies of the out-of-plane C–H vinylenic wag mode ($\sim 966\text{ cm}^{-1}$) with increasing acceptor content, which is expected to be sensitive to chain planarity. Specifically, Bruevich et al. proposed that the dopant interacts preferentially in a face-on manner with the phenylene group and that induce planarity in neighboring segments resulting in blue-shifts and lower relative intensities of the vinylenic CH wag.³⁷ For DDQ doping of MDMO-PPV, the high sensitivity of MDMO-PPV Raman transitions centered on the electron-rich phenylene moiety is consistent with preferential DDQ interactions with this component.

Figure 5 shows the effect of the frequency and integrated intensity as a function of DDQ loading on the $\sim 966\text{ cm}^{-1}$ mode of MDMO-PPV. Raman spectra were again excited with 780 nm light to take advantage of the preresonance enhancement involving the putative MDMO-PPV ordered form. As the DDQ loading increases, the relative integrated intensity of the $\sim 966\text{ cm}^{-1}$ mode decreases and blue-shifts by $\sim 2\text{ cm}^{-1}$ as shown in Figure 5b. These trends are similar to those reported by Bruevich and co-workers³⁷ demonstrating that doping induces coplanarity consistent with the new red-shifted absorption band. However, these authors observed no significant intensity gains of the ~ 1280 and $\sim 1555\text{ cm}^{-1}$ modes as seen here with DDQ charge transfer doping.³⁷

Ground state Raman spectra were also simulated to compare intensities with and without DDQ (see Supporting Information). Distinct transitions corresponding to ionized donor and acceptor forms were observed but not directly comparable to experiment due to resonance enhancement effects. Most importantly, the emergence of resolved overtone-combination transitions under preresonance excitation conditions suggests

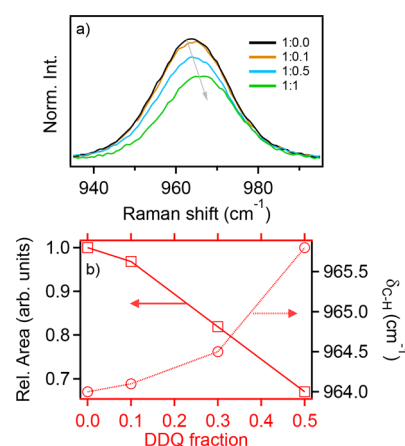


Figure 5. (a) Effect of DDQ loading on the out-of-plane CH vinylenic wag mode. Intensities were normalized to the dominant CC backbone stretching mode ($\sim 1580\text{ cm}^{-1}$) to allow comparison of relative intensity changes incurred. (b) Relative integrated intensities and frequency maxima of the out-of-plane CH vinylenic wag mode.

that these features are unique to the ordered MDMO-PPV form. According to the time-dependent theory of Raman spectroscopy, preresonant excitation conditions only sample a small region of the excited state potential surface near the Franck–Condon region or, in other words, fast dynamics (i.e., less than one vibrational period).⁴⁵ However, significant enhancement may be observed under these conditions, allowing for selective sampling of the doping-induced red-shifted absorption spectrum in Figure 1a. Although the appearance of overtone-combination progressions are consistent with a greater fraction of the MDMO-PPV ordered component, charged species (polarons) also absorb in the NIR region that possibly overlap with the doped absorption spectrum. However, oscillator strengths of these transitions are also comparatively weaker than the new red-shifted absorption band in Figure 1a suggesting their contributions to overtone intensities in preresonance Raman spectra are probably negligible. Instead, the “turn-on” of resolved overtone/composition progressions with charge transfer doping most likely originates from suppressed backbone torsional displacements as well as reduced coupling of the time-dependent Raman wavepacket to the surroundings. Here, we explore these

features in the following by comparing Raman patterns excited on resonance with the pristine and doped MDMO-PPV forms.

Insights into Doping-Induced Enhancement of Chain Planarity and Polaron Delocalization from Resonance Raman Overtones. In many Raman studies of large conjugated organic molecules, overtone and combination bands are usually masked or broadened due to rapid excited state relaxation dynamics caused by strong coupling to extramolecular motions or the involvement of many displaced Franck–Condon active vibrational modes. These effects result in excessive damping or self-cancellation of recurrences in the wavepacket cross-correlation overlap that destroy overtone intensities.⁴⁵ When overtones are resolved, these features encode the specific path(s) the wavepacket traveled on the excited state potential energy surface, which is more conveniently “read-out” in the frequency domain on the ground state potential surface. We now consider the contributions of these factors involved in the appearance of long overtone-combination progressions when MDMO-PPV chains become doped, which can also shed light on the formation of either polarons or bipolarons as observed in EPR spectra.

Figure 6 shows resonance Raman spectra of MDMO-PPV/DDQ (1:1 w/w) thin films excited with 488 nm (2.54 eV) and

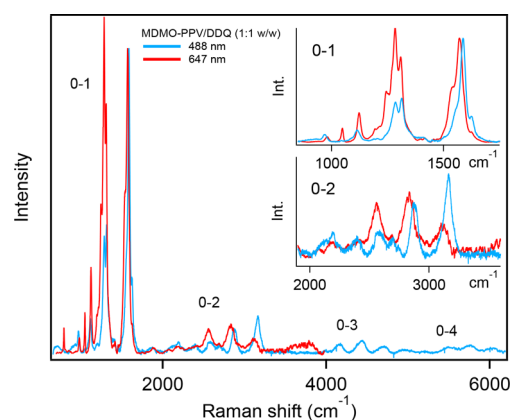


Figure 6. Resonance Raman spectra of MDMO-PPV/DDQ blends excited with 488 nm (blue trace) and 647 nm (red trace) light. Insets highlight the intensity distributions of the fundamental (0–1) and first (0–2) overtone-combination transitions.

647 nm (1.92 eV) light that is resonant with absorption maxima of pristine-like and doped MDMO-PPV chains, respectively. Comparing Raman spectra excited with 780 nm light (Figure 2) to those generated with 647 nm light reveals similar patterns, consistent with selective excitation of the ordered MDMO-PPV variant. Because of greater broadening of the low energy Raman signatures and detector sensitivity limits, it was not possible to record spectra beyond the first overtone region with lower excitation energies. Conversely, higher excitation energies show longer overtone-combination progressions and clusters are dominated by combination transitions involving the high frequency CC skeletal stretching modes discussed earlier. The spectra in Figure 6 are similar to those from our earlier study of MDMO-PPV/DDQ blend thin films of one loading (i.e., 1:1 w/w) and in both cases, several pure overtones (up to four quanta) of the dominant ~ 1580 , ~ 1555 , ~ 1310 , and ~ 1280 cm^{-1} modes are resolved.³¹ Comparison between the intensity distributions of the fundamental and overtone replicas for both

excitation energies reveals two distinct patterns consistent with structurally distinct MDMO-PPV forms. Because 488 nm excitation preferentially excites pristine-like MDMO-PPV chains, there are clearly a significant fraction of monomers or segments that either interact weakly with DDQ or do not become doped.

The fact that overtone-combination transitions do not appear until the polymer becomes doped indicates that the ordered MDMO-PPV form dominates these features. This is supported by the evolution of Raman patterns from preresonance excitation (Figure 2) that clearly show the emergence of the characteristic overtone-combination clusters observed in Figure 6. Furthermore, the ~ 1280 and ~ 1555 cm^{-1} modes dominate intensity contributions to overtone-combination progressions beyond the 0–2 region which show the greatest activity when MDMO-PPV chains are converted to the ordered form via doping. This is expected since overtone-combination intensities develop at later times consistent with either larger displacements or long-lived wavepacket motion involving the ordered form.⁴⁶ Interestingly, overtone-combination intensities are less prominent in resonance Raman spectra of MDMO-PPV chains blended with weak acceptors (e.g., fullerenes) that do not promote conversion to the ordered conformer (see Supporting Information).

Considering the dominant contributing modes, namely, the ~ 1280 and 1555 cm^{-1} CC stretching modes, have vibrational periods of ca. 20–30 fs suggests that this lifetime must be on the order of ~ 100 fs. Recent stimulated resonance Raman spectroscopy studies using ultrashort pulsed excitation of MDMO-PPV blended with fullerene acceptors demonstrated that these particular modes dominate the observed exciton dynamics up to ~ 1 ps.⁴⁶ Hoffman et al. attributed these vibrations to the MDMO-PPV cation (MDMO-PPV⁺), consistent with significant quinoidal character when chains are doped.⁴⁶ The appearance of multiple harmonics in MDMO-PPV with doping in Figure 6 also demonstrate multiple return visits of the time-dependent wavepacket and suppressed anharmonic coupling on ~ 100 fs time scales or less. Furthermore, we expect the broader line widths of these transitions reflect a distribution of conjugation lengths suggesting larger region of the polymer backbone is sampled during the excited state lifetime.

The appearance of long overtone progressions in doped MDMO-PPV chains and distinct resonances in EPR spectra corresponding to uncorrelated holes and electrons are consistent with the delocalized nature of these segments. As dopant loadings increase, stiffening of adjacent MDMO-PPV chain segments occurs that allows polarons to delocalize further but, as more carriers are injected, there is an increasing likelihood that carrier–carrier interactions (i.e., superexchange coupling) will begin to affect these spins. This regime is apparent from EPR signals from the reduction in the hole polaron resonance marks the onset of bipolaron formation (see Figure 1c) where the resonance assigned to hole polarons ($g = \sim 2.0085$) decreases with respect to the dopant anion ($g = \sim 2.0065$). Resonance excitation profiles are next measured that are useful for sorting out the presence of multiple conformers and we use this information to identify vibrational modes supporting polaronic character.

Figure 7 displays excitation profiles for MDMO-PPV/DDQ (1:1 w/w) thin films generated with excitation energies spanning the entire absorption bandwidth in Figure 1a. We do not attempt to quantitatively estimate absolute Raman

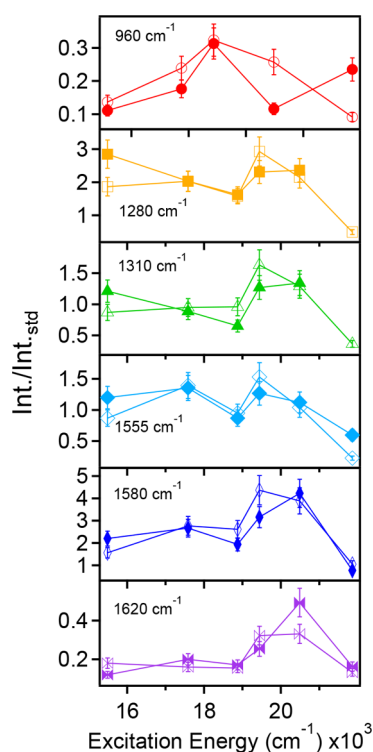


Figure 7. Resonance Raman excitation profiles of the main skeletal vibrations of MDMO-PPV in a 1:1 w/w blend with DDQ. Solid symbols correspond to as-cast thin films and open symbols correspond to annealed thin films.

scattering cross sections of both forms, however, these profiles are used to reveal vibrational modes that derive intensity from a particular conformer, i.e., from the pristine-like chain and doped segments. If only one electronic transition with substantial oscillator strength dominates the absorption spectrum then profiles tend to resemble these line shapes. It is for this reason that Raman excitation profiles are more advantageous probes of specific conformers since Raman intensities of a single mode can be investigated as a function of excitation energy to expose state-specific contributions. Only the main skeletal vibrations of the MDMO-PPV backbone are targeted in Figure 7 and qualitative inspection reveals that Raman signatures originate from at least two structurally distinct species. For example, concentrating on the high frequency C=C stretching region of the MDMO-PPV backbone (~ 1555 – 1620 cm^{-1}), there is an apparent shift in the relative excitation efficiency toward the higher energy form when comparing ~ 1555 , ~ 1580 , and 1620 cm^{-1} modes, respectively. Here, the ~ 1555 cm^{-1} mode shows nearly equal contributions from both forms whereas the ~ 1580 and ~ 1620 cm^{-1} modes exhibit greater excitation efficiency from the pristine-like form. Similar comparisons with the inter-ring CC stretches (i.e., ~ 1280 and ~ 1310 cm^{-1}) are less straightforward to interpret due to their smaller separation and larger line widths.

It is also interesting to note that the out-of-plane vinylene CH wag mode (~ 960 cm^{-1}) mode shows no significant dependence on either form. This could be the result of its lower relative intensity which can make it difficult to accurately resolve excitation efficiencies of multiple structures whose electronic absorption spectra overlap significantly. Nonetheless, the effect of DDQ loading on the intensity and frequency of

this mode do in fact show evidence of increased planarity (i.e., intensity decreases and blue-shifts, see Figure 5) which leads us to conclude it should have a lower excitation efficiency as a larger fraction of chains convert to the ordered form. In addition, the appearance of “dips” in several profiles (in particular, 1280, 1310, and 1555 cm^{-1} modes) at ca. 19 000 cm^{-1} coincide almost exactly to the observed isosbestic point observed in MDMO-PPV/DDQ absorption spectra in Figure 1. We attribute this feature, as well as the nonuniform excitation efficiency for the higher frequency CC stretches, to the manner in which DDQ molecules interact with the PPV backbone. Specifically, vibrational modes of mostly phenylene stretching character show selective excitation behavior whereas those of inter-ring vibrations are less affected. This result confirms that the DDQ dopants interact preferentially with the phenylene group.

We next investigated the effect of thermal annealing of doped MDMO-PPV thin films which may further perturb the relative amounts of ordered and pristine-like chains. Thermal annealing treatments may therefore reveal the relative stability of MDMO-PPV conformers and possible dedoping, which has been demonstrated by exposing doped films to light.⁴⁷ Doped thin films were heated to ~ 120 $^{\circ}\text{C}$ for ~ 10 min and corresponding excitation profiles are displayed as open symbols in Figure 7. Overall, no significant changes in Raman intensities are observed with varying excitation energies indicating conformational stability.

Lastly, Raman spectroscopy is used frequently to understand both structural and electronic properties of conjugated polymers in both neutral and charged states. The archetype Raman pattern of alkoxy substituted PPV derivatives (represented by the pristine spectrum in Figure 2) has always been interpreted in terms of a single chromophore and normal coordinate assignments were based largely on the overall similarity to stilbenes and unsubstituted PPV.⁴⁸ We now believe that the pristine Raman pattern actually contains signatures of two structurally distinct conformers, which was demonstrated by selecting out the ordered form by charge transfer doping. The fact that the ordered form is a minority species in the neat material has masked its identity from Raman measurements although single molecule spectroscopy studies have been able to resolve both species due to greater sensitivity and disrupting rapid energy funneling by dilution.^{29,30}

Figure 8 shows Raman spectra of the two MDMO-PPV components with the ordered form generated via charge transfer doping. It is important to stress that this line shape is not an exact representation of the ordered form in the pristine material because of red-shifts and broadening incurred upon

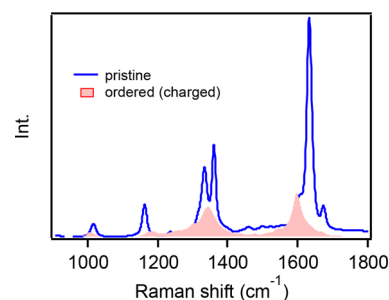


Figure 8. Raman spectra of pristine and the ordered (charged) MDMO-PPV structures.

doping. However, as shown in Figure 2, the sensitivity of this line shape to dopant loading confirms its role as a polaron precursor.

CONCLUSIONS

Charge transfer doping of the nominally disordered MDMO-PPV polymer induces ordering (stiffening) of chain segments leading to new absorption and Raman spectral signatures. Doping is facilitated by the presence of a minority ordered form, which acts as a precursor for hole polarons due to lower reorganization barriers for delocalizing injected holes away from the charge transfer site. Furthermore, charge injection induces stiffening on neighboring segments that effectively increases the relative amounts of the ordered form. We propose that these structures also lead to formation of spinless bipolarons at larger dopant loadings, which are EPR silent. The delocalized nature of the ordered (doped) MDMO-PPV form is perhaps most apparent from long progressions of overtone-combination transitions involving the dominant displaced CC backbone stretching modes. Theoretical simulations support this view and demonstrate a larger fraction of charge transfer as chain lengths increase as well as distinct quinoidal distortions upon doping. We propose that careful choice of dopants and processing could potentially be harnessed to control carrier levels and charge transport in a more reliable fashion than available from conventional processing approaches.

ASSOCIATED CONTENT

Supporting Information

The Supporting Information is available free of charge on the ACS Publications website at DOI: 10.1021/acs.jpcc.7b08773.

Absorption spectra of MDMO-PPV/DDQ solutions, absorption spectrum of MDMO-PPV cast from a high boiling point solvent, theoretical spectra of DDQ and DDQ anion, and resonance Raman spectra of MDMO-PPV with weak and strong acceptors (PDF)

AUTHOR INFORMATION

Corresponding Author

*(J.K.G.) jkgrey@unm.edu

ORCID

Martin L. Kirk: 0000-0002-1479-3318

Hua Guo: 0000-0001-9901-053X

John K. Grey: 0000-0001-7307-8894

Present Address

[†]Los Alamos National Laboratory, Los Alamos, NM 87545

Notes

The authors declare no competing financial interest.

ACKNOWLEDGMENTS

J.K.G. and M.L.K. acknowledge the National Science Foundation (NSF CHE 1506558 and NSF CHE 1301142 and NSF #IIA-1301346, respectively) for financial assistance.

REFERENCES

- (1) Walzer, K.; Maennig, B.; Pfeiffer, M.; Leo, K. Highly Efficient Organic Devices Based on Electrically Doped Transport Layers. *Chem. Rev.* **2007**, *107*, 1233–1271.
- (2) Luessem, B.; Riede, M.; Leo, K. Doping of Organic Semiconductors. *Phys. Status Solidi A* **2013**, *210*, 9–43.

- (3) Aziz, E. F.; Vollmer, A.; Eisebitt, S.; Eberhardt, W.; Pingel, P.; Neher, D.; Koch, N. Localized Charge Transfer in a Molecularly Doped Conducting Polymer. *Adv. Mater.* **2007**, *19*, 3257–3260.

- (4) Lussem, B.; Keum, C.-M.; Kasemann, D.; Naab, B.; Bao, Z.; Leo, K. Doped Organic Transistors. *Chem. Rev.* **2016**, *116*, 13714–13751.

- (5) Scholes, D. T.; Hawks, S. A.; Yee, P. Y.; Wu, H.; Lindemuth, J. R.; Tolbert, S. H.; Schwartz, B. J. Overcoming Film Quality Issues for Conjugated Polymers Doped with F4tcnq by Solution Sequential Processing: Hall Effect, Structural, and Optical Measurements. *J. Phys. Chem. Lett.* **2015**, *6*, 4786–4793.

- (6) Bredas, J. L.; Street, G. B. Polarons, Bipolarons, and Solitons in Conducting Polymers. *Acc. Chem. Res.* **1985**, *18*, 309–15.

- (7) Koch, N.; Rajagopal, A.; Ghijsen, J.; Johnson, R. L.; Leising, G.; Pireaux, J. J. Bipolaron. The Stable Charged Species in N-Doped P-Sexiphenyl. *J. Phys. Chem. B* **2000**, *104*, 1434–1438.

- (8) Furukawa, Y. Electronic Absorption and Vibrational Spectroscopies of Conjugated Conducting Polymers. *J. Phys. Chem.* **1996**, *100*, 15644–15653.

- (9) Koch, N.; Leising, G.; Yu, L. M.; Rajagopal, A.; Pireaux, J. J.; Johnson, R. L. Bipolaron Formation in Para-Sexiphenyl Thin Films Upon Cs Doping. *J. Vac. Sci. Technol., A* **2000**, *18*, 295–298.

- (10) Salzmann, I.; Heimel, G.; Oehzelt, M.; Winkler, S.; Koch, N. Molecular Electrical Doping of Organic Semiconductors: Fundamental Mechanisms and Emerging Dopant Design Rules. *Acc. Chem. Res.* **2016**, *49*, 370–378.

- (11) Pingel, P.; Neher, D. Comprehensive Picture of P-Type Doping of P3ht with the Molecular Acceptor F4TCNQ. *Phys. Rev. B: Condens. Matter Mater. Phys.* **2013**, *87*, 115209.

- (12) Mendez, H.; Heimel, G.; Winkler, S.; Frisch, J.; Opitz, A.; Sauer, K.; Wegner, B.; Oehzelt, M.; Roethel, C.; Duhm, S.; et al. Charge-Transfer Crystallites as Molecular Electrical Dopants. *Nat. Commun.* **2015**, *6*, 8560.

- (13) Mendez, H.; Heimel, G.; Opitz, A.; Sauer, K.; Barkowski, P.; Oehzelt, M.; Soeda, J.; Okamoto, T.; Takeya, J.; Arlin, J. B.; et al. Doping of Organic Semiconductors: Impact of Dopant Strength and Electronic Coupling. *Angew. Chem., Int. Ed.* **2013**, *52*, 7751–7755.

- (14) Fuzell, J.; Jacobs, I. E.; Ackling, S.; Harrelson, T. F.; Huang, D. M.; Larsen, D.; Moule, A. J. Optical Dedoping Mechanism for P3ht:F4tcnq Mixtures. *J. Phys. Chem. Lett.* **2016**, *7*, 4297–4303.

- (15) Gao, J.; Niles, E. T.; Grey, J. K. Aggregates Promote Efficient Charge Transfer Doping of Poly(3-Hexylthiophene). *J. Phys. Chem. Lett.* **2013**, *4*, 2953–2957.

- (16) Cochran, J. E.; Junk, M. J. N.; Gludell, A. M.; Miller, P. L.; Cowart, J. S.; Toney, M. F.; Hawker, C. J.; Chmelka, B. F.; Chabiny, M. L. Molecular Interactions and Ordering in Electrically Doped Polymers: Blends of PBTtT and F4TCNQ. *Macromolecules* **2014**, *47*, 6836–6846.

- (17) Di Nuzzo, D.; Fontanesi, C.; Jones, R.; Allard, S.; Dumsch, I.; Scherf, U.; von Hauff, E.; Schumacher, S.; Da Como, E. How Intermolecular Geometrical Disorder Affects the Molecular Doping of Donor-Acceptor Copolymers. *Nat. Commun.* **2015**, *6*, 6460.

- (18) Di Pietro, R.; Erdmann, T.; Wang, N.; Liu, X.; Grafe, D.; Lenz, J.; Brandt, J.; Kasemann, D.; Leo, K.; Al-Hussein, M.; et al. The Impact of Molecular Weight, Air Exposure and Molecular Doping on the Charge Transport Properties and Electronic Defects in Dithienyl-Diketopyrrolopyrrole-Thieno[3,2-B]Thiophene Copolymers. *J. Mater. Chem. C* **2016**, *4*, 10827–10838.

- (19) Gao, J.; Stein, B. W.; Thomas, A. K.; Garcia, J. A.; Yang, J.; Kirk, M. L.; Grey, J. K. Enhanced Charge Transfer Doping Efficiency in J-Aggregate Poly(3-Hexylthiophene) Nanofibers. *J. Phys. Chem. C* **2015**, *119*, 16396–16402.

- (20) Harrelson, T. F.; Cheng, Y. Q.; Li, J.; Jacobs, I. E.; Ramirez-Cuesta, A. J.; Faller, R.; Moule, A. J. Identifying Atomic Scale Structure in Undoped/Doped Semicrystalline P3HT Using Inelastic Neutron Scattering. *Macromolecules* **2017**, *50*, 2424–2435.

- (21) Karpov, Y.; Erdmann, T.; Raguzin, I.; Al-Hussein, M.; Binner, M.; Lappan, U.; Stamm, M.; Gerasimov, K. L.; Beryozkina, T.; Bakulev, V.; et al. High Conductivity in Molecularly P-Doped Diketopyrrolopyrrole-Based Polymer: The Impact of a High Dopant

Strength and Good Structural Order. *Adv. Mater.* **2016**, *28*, 6003–6010.

(22) McFarland, F. M.; Bonnette, L. R.; Acres, E. A.; Guo, S. The Impact of Aggregation on the P-Doping Kinetics of Poly(3-Hexylthiophene). *J. Mater. Chem. C* **2017**, *5*, 5764–5771.

(23) Mueller, L.; Nanova, D.; Glaser, T.; Beck, S.; Pucci, A.; Kast, A.; Schroeder, R.; Mankel, E.; Pingel, P.; Neher, D.; et al. Charge-Transfer-Solvent Interaction Predefines Doping Efficiency in P-Doped P3HT Films. *Chem. Mater.* **2016**, *28*, 4432–4439.

(24) Olthof, S.; Tress, W.; Meerheim, R.; Luessem, B.; Leo, K. Photoelectron Spectroscopy Study of Systematically Varied Doping Concentrations in an Organic Semiconductor Layer Using a Molecular P-Dopant. *J. Appl. Phys.* **2009**, *106*, 103711.

(25) Duong, D. T.; Phan, H.; Hanifi, D.; Jo, P. S.; Nguyen, T.-Q.; Salleo, A. Direct Observation of Doping Sites in Temperature-Controlled, P-Doped P3HT Thin Films by Conducting Atomic Force Microscopy. *Adv. Mater.* **2014**, *26*, 6069–6073.

(26) Pingel, P.; Schwarzl, R.; Neher, D. Effect of Molecular P-Doping on Hole Density and Mobility in Poly(3-Hexylthiophene). *Appl. Phys. Lett.* **2012**, *100*, 143303.

(27) Duong, D. T.; Wang, C.; Antono, E.; Toney, M. F.; Salleo, A. The Chemical and Structural Origin of Efficient P-Type Doping. *Org. Electron.* **2013**, *14*, 1330–1336.

(28) Yoon, S.; Cho, J.; Lee, H.-K.; Park, S.; Son, H. J.; Chung, D. S. Effects of 2,3,5,6-Tetrafluoro-7,7,8,8-Tetracyanoquinodimethane Doping on Diketopyrrolopyrrole-Based, Low Crystalline, High Mobility Polymeric Semiconductor. *Appl. Phys. Lett.* **2015**, *107*, 133302.

(29) Barbara, P. F.; Gesquiere, A. J.; Park, S.-J.; Lee, Y. J. Single-Molecule Spectroscopy of Conjugated Polymers. *Acc. Chem. Res.* **2005**, *38*, 602–610.

(30) Huser, T.; Yan, M.; Rothberg, L. J. Single Chain Spectroscopy of Conformational Dependence of Conjugated Polymer Photophysics. *Proc. Natl. Acad. Sci. U. S. A.* **2000**, *97*, 11187–11191.

(31) Wise, A. J.; Grey, J. K. Resonance Raman Studies of Excited State Structural Displacements of Conjugated Polymers in Donor/Acceptor Charge Transfer Complexes. *Phys. Chem. Chem. Phys.* **2012**, *14*, 11273–11276.

(32) Favors, R. N.; Jiang, Y.; Loethen, Y. L.; Ben-Amotz, D. External Raman Standard for Absolute Intensity and Concentration Measurements. *Rev. Sci. Instrum.* **2005**, *76*, 033108.

(33) Grimme, S. Semiempirical GGA-Type Density Functional Constructed with a Long-Range Dispersion Correction. *J. Comput. Chem.* **2006**, *27*, 1787–1799.

(34) Becke, A. D.; Johnson, E. R. A Density-Functional Model of the Dispersion Interaction. *J. Chem. Phys.* **2005**, *123*, 154101.

(35) Weigend, F.; Ahlrichs, R. Balanced Basis Sets of Split Valence, Triple Zeta Valence and Quadruple Zeta Valence Quality for H to Rn: Design and Assessment of Accuracy. *Phys. Chem. Chem. Phys.* **2005**, *7*, 3297–3305.

(36) Neese, F.; Wennmohs, F.; Hansen, A.; Becker, U. Efficient, Approximate and Parallel Hartree-Fock and Hybrid DFT Calculations. A 'Chain-of-Spheres' Algorithm for the Hartree-Fock Exchange. *Chem. Phys.* **2009**, *356*, 98–109.

(37) Bruevich, V. V.; Makhmutov, T. S.; Elizarov, S. G.; Nechvolodova, E. M.; Paraschuk, D. Y. Raman Spectroscopy of Intermolecular Charge Transfer Complex between a Conjugated Polymer and an Organic Acceptor Molecule. *J. Chem. Phys.* **2007**, *127*, 104905.

(38) Paraschuk, O. D.; Bruevich, V. V.; Paraschuk, D. Y. Association Function of Conjugated Polymer Charge-Transfer Complex. *Phys. Chem. Chem. Phys.* **2010**, *12*, 6021–6026.

(39) Bruevich, V. V.; Makhmutov, T. S.; Elizarov, S. G.; Nechvolodova, E. M.; Paraschuk, D. Y. Raman Spectroscopy of Intermolecular Charge Transfer Complex between a Conjugated Polymer and an Organic Acceptor Molecule. *J. Chem. Phys.* **2007**, *127*, 104905.

(40) Huber, R. C.; Ferreira, A. S.; Thompson, R.; Kilbride, D.; Knutson, N. S.; Devi, L. S.; Toso, D. B.; Challa, J. R.; Zhou, Z. H.; Rubin, Y.; et al. Long-Lived Photoinduced Polaron Formation in

Conjugated Polyelectrolyte-Fullerene Assemblies. *Science* **2015**, *348*, 1340–1343.

(41) Koehler, A.; Hoffmann, S. T.; Baessler, H. An Order-Disorder Transition in the Conjugated Polymer MeH-Ppv. *J. Am. Chem. Soc.* **2012**, *134*, 11594–11601.

(42) Sakamoto, A.; Furukawa, Y.; Tasumi, M.; Noguchi, T.; Ohnishi, T. Resonance Raman Spectra of SO₃-Doped Poly(P-Phenylenevinylene). *Synth. Met.* **1995**, *69*, 439–40.

(43) Sakamoto, A.; Furukawa, Y.; Tasumi, M. Spectroscopic Studies on the Radical-Cation Dimer of a Model Compound of Poly(P-Phenylenevinylene). Similarities between the Dimer and the State of Positive Polarons in the Sulfuric-Acid-Treated Polymer. *J. Phys. Chem. B* **1997**, *101*, 1726–1732.

(44) Honda, K.; Furukawa, Y.; Furuya, K.; Torii, H.; Tasumi, M. Density Functional Theory Study on the Raman Spectra of Negative Polarons and Negative Bipolarons in Na-Doped Poly(P-Phenylene). *J. Phys. Chem. A* **2002**, *106*, 3587–3592.

(45) Tannor, D. J.; Heller, E. J. Polyatomic Raman Scattering for General Harmonic Potentials. *J. Chem. Phys.* **1982**, *77*, 202–18.

(46) Hoffman, D. P.; Leblebici, S. Y.; Schwartzberg, A. M.; Mathies, R. A. Exciton Mobility in Organic Photovoltaic Heterojunctions from Femtosecond Stimulated Raman. *J. Phys. Chem. Lett.* **2015**, *6*, 2919–2923.

(47) Jacobs, I. E.; Wang, F.; Hafezi, N.; Medina-Plaza, C.; Harrelson, T. F.; Li, J.; Augustine, M. P.; Mascall, M.; Moule, A. J. Quantitative Dedoping of Conductive Polymers. *Chem. Mater.* **2017**, *29*, 832–841.

(48) Furukawa, Y.; Sakamoto, A.; Tasumi, M. Raman and Infrared Studies on the Molecular Structures of Poly(1,4-Phenylenevinylene) and Poly(2,5-Thienylenevinylene). *J. Phys. Chem.* **1989**, *93*, 5354–6.